Astronomy & Astrophysics manuscript no. 0683xmmh February 2, 2008
(DOI: will be inserted by hand later)

XMM-Newton spectra of hard spectrum *Rosat* AGN: X–ray absorption and optical reddening

F.J. Carrera[1], M.J. Page[2], and J.P.D. Mittaz[3]

[1] Instituto de Física de Cantabria (CSIC-UC), Avenida de los Castros, 39005 Santander (Spain)
e-mail: carreraf@ifca.unican.es
[2] Mullard Space Science Laboratory-University College London, Surrey RH5 6NT, United Kingdom
e-mail: mjp@mssl.ucl.ac.uk
[3] University of Huntsville, Alabama, United States e-mail: mittazj@email.uah.edu

Received November 15, 2003; accepted March 3, 2004

Abstract. We present the *XMM-Newton* spectra of three low-redshift intermediate Seyferts (one Sy1.5, and two Sy1.8), from our survey of hard spectrum *Rosat* sources. The three AGN are well fitted by absorbed powerlaws, with intrinsic nuclear photoelectric absorption from column densities between 1.3 and 4.0 $\times 10^{21}$ cm^{-2}. In the brightest object the X–ray spectrum is good enough to show that the absorber is not significantly ionized. For all three objects the powerlaw slopes appear to be somewhat flatter ($\Gamma \sim 1.3 - 1.6$) than those found in typical unabsorbed Seyferts. The constraints from optical and X–ray emission lines imply that all three objects are Compton-thin. For the two fainter objects, the reddening deduced from the optical broad emission lines in one of them, and the optical continuum in the other, are similar to those expected from the X–ray absorption, if we assume a Galactic gas-to-dust ratio and reddening curve. The broad line region Balmer decrement of our brightest object is larger than expected from its X–ray absorption, which can be explained either by an intrinsic Balmer decrement with standard gas-to-dust ratio, or by a >Galactic gas-to-dust ratio. These ≥ Galactic ratios of extinction to photoelectric absorption cannot extend to the high redshift, high luminosity, broad line AGN in our sample, because they have column densities > 10^{22} cm^{-2}, and so their broad line regions would be totally obscured. This means that some effect (e.g., luminosity dependence, or evolution) needs to be present in order to explain the whole population of absorbed AGN.

Key words. Galaxies: active – Galaxies: Seyfert – quasars: emission lines – X-rays: galaxies

1. Introduction

According to the unified model for Active Galactic Nuclei (AGN)(Antonucci 1993), broad-line Seyferts (type 1) and narrow-line (type 2) Seyferts are intrinsically the same type of object but are viewed with different orientations to our line of sight. In this model the central engine of the AGN, and the high velocity clouds that produce the broad optical and UV emission lines, are surrounded by a thick torus of dust and cool, molecular gas. In type 1 objects we have a direct view of the central engine and the broadline clouds, whereas in type 2 objects the torus blocks our line of sight to these regions. Such a torus has a large photoelectric opacity at soft X–ray energies, which explains why type 1 Seyferts have steep X–ray spectra with little absorption (Nandra & Pounds 1994), and type 2 Seyferts have absorbed X–ray spectra (Smith & Done 1996). Narrow emission lines are produced in more distant gas clouds on scales larger than the dusty torus, and so can be seen in both types of object. Objects in which the broad lines are attenuated, but not completely obscured, are called intermediate Seyferts, and are assigned classifications ranging from 1.5-1.9.

However, even in the type 1 objects, an extra absorption component from ionized gas is often seen in the X–ray band (George et al. 1998). This ionized gas, the "warm absorber", appears to be distributed throughout the BLR and NLR of Seyfert galaxies, and in type 2 objects it can scatter nuclear radiation into our line of sight. The warm absorber has a much lower opacity to soft X–rays than cold gas, but if it contains a significant element of dust (e.g. Brandt, Fabian & Pounds 1996) it could produce considerable extinction at optical and ultraviolet wavelengths.

An understanding of absorption in AGN is extremely important. For example, unified AGN models for the X–ray background (XRB) (see e.g., Setti & Woltjer 1989, for an early proposal, and Gilli, Salvati & Hasinger 2001, for a late development) explain the spectrum of the XRB by the superposition of spectra of AGN with various degrees of absorption. Under this scheme, soft spectrum X–ray sources should be mostly type 1 AGN, while hard spectrum X–ray sources would be predominantly type 2 AGN. In the 1990s this matched the observations quite well, because *Rosat* surveys in the soft band were dominated by type 1 AGN, (e.g. Mason et al. 2000, Lehman et al.

2001) while surveys selected in harder bands with *BeppoSAX* (Fiore et al. 1999) were much richer in type 2 AGN.

Despite these early successes, recent developments have put in jeopardy the identity between optical type 1 and X–ray unabsorbed objects, on one hand, and optical type 2 and X–ray absorbed objects, on the other. For example, identifications of our survey of *Rosat* sources with hard spectra (Page, Mittaz & Carrera 2000, 2001) produced mostly type 1 AGN, contrary to the expectations of the unified model. Other examples of X–ray absorbed type 1 objects have been found by Akiyama et al. (2000) using *ASCA* data, and Mainieri et al. (2002) and Page et al. (2003) using *XMM-Newton* data. In principle, high gas-to-dust ratios in the X–ray absorbing gas (perhaps due to dust sublimation close to the central X–ray source, Granato, Danese & Franceschini 1997), or large dust grains (Maiolino, Marconi & Oliva 2001), could give rise to high levels of X–ray absorption, without much optical obscuration.

In the opposite sense, Pappa et al. (2001) have found several examples of type 2 AGN with very little or no X–ray absorption. Panessa & Bassani (2002) estimate that 10-30% of Seyfert 2 galaxies have this property. One striking example is H1320+551 (Barcons, Carrera & Ceballos 2003), a Seyfert 1.8/1.9 galaxy with strong optical (BLR and NLR) obscuration, but without any corresponding X–ray absorption from cold gas. The high quality of their *XMM-Newton* data allows these authors to rule out a warm absorber in this source, which leads them to the conclusion that the BLR is intrinsically reddened in this object: its Sy 1.8/1.9 appearance cannot arise from obscuration of a Seyfert 1 spectrum.

The situation is therefore complex. Possible explanations include Compton thick obscuration which could suppress completely the nuclear emission below 10 keV. This spectral range could then be filled by X–rays scattered off the warm absorber, or by extranuclear emission, which would not have in principle a particularly hard or absorbed spectrum. This could result in optically obscured type 2 AGN which appear to be absorption free at X–ray energies. Such a model can in principle be tested, since Bassani et al. (1999) have developed a diagnostic diagram that permits identifying Compton thick sources, as those with high equivalent width Fe emission lines (originating in fluorescence in the torus material), and low 2-10 keV to [OIII] flux ratio. This is based on the observation that [OIII] originates in the NLR, outside the torus, and thus in principle [OIII] should be free of obscuration. Neither H1320+551, nor any of the sources discussed in Pappa et al. (2001), lie in the Compton thick region of this diagram. They represent therefore genuine mismatches between optical and X–ray classifications, at odds with the unified AGN model.

Here, we analyze optical and *XMM-Newton* spectroscopic data on three AGN (RXJ133152.51+111643.5, RXJ163054.25+781105.1, and RXJ213807.61-423614.3) from the sample of Page, Mittaz & Carrera (2001). Of the objects in this sample which show broad optical emission lines, these three had the highest X–ray fluxes. All three show strong signs of absorption in their *Rosat* spectra. In section 2 we present their optical spectra, finding evidence for optical obscuration in at least two of them. We then analyze their *XMM-Newton* spectra in section 3, and in particular we measure their intrinsic X–ray absorption. The differences between the levels of optical obscuration and X–ray absorption are discussed in section 4, as well as a comparison of the X–ray spectral properties of our sources with respect to those of other samples at similar flux levels. Finally, in section 4 we summarize our results.

For brevity, we will refer to the three sources using truncated versions of their names (i.e. RXJ1331, RXJ1630 and RXJ2138) in the text. We have used the currently fashionable values of $H_0 = 70$ km s^{-1} Mpc^{-1}, $\Omega_m = 0.3$, and $\Omega_\Lambda = 0.7$, throughout this paper.

2. Optical spectra

The three sources in this study were taken from the Page, Mittaz & Carrera (2001) sample of sources with hard *Rosat* spectra. One of them (RXJ2138) was identified as an AGN at $z = 0.019$ during the follow-up programme for that project. For this optical spectrum we make use of the photon statistical errors which were propagated through the data reduction. The other two objects (RXJ1331 and RXJ1630) were identified during the RIXOS project (Mason et al. 2000), as AGN at $z = 0.090$ and $z = 0.358$ respectively, and we have taken the optical spectra from the archive of that project. For these two spectra, statistical errors are not available, so we have estimated the statistical uncertainties from the dispersion of the data around a straight line in an emission-line-free continuum region. We have estimated the confidence intervals on the fitted parameters using the standard $\Delta\chi^2$ technique. Given the low resolution of the spectra, in all the fits the relative central wavelengths of the lines with respect to $H\beta$ have been fixed to their rest values. We have assumed that for each object, all the narrow lines have the same width, and similarly for the broad lines, to keep the number of independent parameters to a minimum.

The optical reddening can be calculated using $E(B-V) = 2.07\log((\mathrm{H}\alpha/\mathrm{H}\beta)/(\mathrm{H}\alpha/\mathrm{H}\beta)_{\mathrm{intrinsic}})$ (Osterbrock 1989), where the intrinsic Balmer decrements are 3 for the NLR and 3.43±0.19 for the BLR (see appendix A). Assuming a standard gas-to-dust ratio, the total Hydrogen (HI+H_2) column density is then given by $N_H = 5.8\times10^{21}E(B-V)$ cm^{-2} (Bohlin, Savage & Drake 1978). We have added in quadrature an additional 10% uncertainty on the Balmer decrements, to take into account possible relative flux calibration differences over large ranges of the spectra.

We have also compared the broad-band optical spectral shape of RXJ1630 (for which no BLR Balmer decrement can be obtained) with that of the composite QSO spectrum from Francis (2003), with some contribution from a galaxy continuum (in our case we have tried an ES0 from the Coleman, Wu & Weedman 1980 model). See appendix A for a discussion on this technique.

A more detailed analysis of the optical spectra of the three sources follows. The best fit parameters are summarized in Table 1.

Table 1. Summary of parameters from fits to optical spectra. All errors quoted are 1σ for 1 d.o.f. The [OIII] line referred to is at a rest wavelength of 5007Å. The columns marked $E(B-V)$ give the optical reddening from the Balmer decrement, except for the one marked * which is from broad-band properties(see text), with the Galactic reddening subtracted in all cases.

Source	z	Narrow lines					Broad lines			
		σ (Å)	Intensity (10^{-15} erg cm^{-2} s^{-1})			$E(B-V)$ (mag)	σ (Å)	Intensity (10^{-15} erg cm^{-2} s^{-1})		$E(B-V)$ (mag)
			Hβ	[OIII]	Hα			Hβ	Hα	
RXJ1331	0.090 ± 0.004	6.5	9.1±0.3	$101.5^{+0.2}_{-0.4}$	$31.6^{+0.2}_{-0.4}$	0.10 ± 0.04	75.2	$20^{+1.2}_{-1.1}$	$239.74^{+0.03}_{-0.05}$	1.10 ± 0.07
RXJ2138	0.019 ± 0.004	6.3	$1.14^{+0.15}_{-0.17}$	$2.1^{+0.15}_{-0.16}$	$3.4^{+0.11}_{-0.17}$	−0.05 ± 0.12	83	$3.9^{+0.5}_{-0.6}$	$25.8^{+0.3}_{-0.6}$	0.60 ± 0.14
RXJ1630	0.358 ± 0.003	7.9	0.11±0.03	$1.36^{+0.03}_{-0.02}$	-	-	107	$1.98^{+0.10}_{-0.09}$	-	0.00±0.17*

2.1. RXJ133152.51+111643.5

The optical spectrum was taken from the RIXOS project. It was observed using the Faint Object Spectrograph (FOS) on the INT in February 1994 (see Mason et al. 2000 for details). The spectrum is shown in Fig. 1, along with the best fit model to the 5000-7500Å region including a linear continuum, narrow Gaussian lines for Hβ, [OIII]$\lambda\lambda$4959,5007, Hα, [NII]$\lambda\lambda$6584,6548 and [SII]$\lambda\lambda$6731,6717, and additional broad Gaussian lines for Hα and Hβ. The region used to estimate the error bars was 5800-6400Å. The fit is reasonable, with no obvious residuals around Hα or Hβ. The broad component of Hβ does not look very compelling to the eye, but it improves the fit very significantly ($\Delta\chi^2 = 196$ for 298 d.o.f. with just one more parameter). We therefore classify this source as a Sy1.8, instead of the Sy1.9 classification given in Mason et al. (2000). In addition to the above lines, [OII], Hγ and perhaps [NeV] can be distinguished in the spectrum.

The Balmer decrement for the narrow H lines is 3.47 ± 0.16, or $E(B-V) = 0.10 \pm 0.04$ (with the Galactic reddening of 0.03 already subtracted). The NLR is only very slightly reddened. In contrast, the Balmer decrement for the broad H lines is 12 ± 0.7, or $E(B-V) = 1.10 \pm 0.07$ mag (which corresponds to $N_H = (6.4 \pm 0.4) \times 10^{21}$ cm^{-2}, more than 50% higher than the value inferred from the X-ray spectrum, see section 3.1). The BLR appears therefore to be substantially reddened.

The [OIII]5007 flux (which will be used to check if the source is Compton thick in section 3.1) has been determined using the NLR Balmer decrement to correct the [OIII]5007 line intensity for reddening. Following Bassani et al. (1999) and Pappa et al. (2001), we correct the observed [OIII] flux by a factor $[(\mathrm{H}\alpha/\mathrm{H}\beta)_{\rm NLR}/3]^{2.94}$, obtaining $(1.6\pm0.3)\times10^{-13}$ erg cm^{-2} s^{-1}. Because our spectrum was taken through a narrow slit with relatively inaccurate absolute photometry, we have applied a correction to the [OIII]5007 flux. We obtained a correction factor of 0.53 ± 0.07 by comparing the flux in the spectrum with our CCD photometry (R=16.45±0.06, Carrera, Page & Stevens 2003), and hence obtain a final value of $(0.85 \pm 0.19) \times 10^{-13}$ erg cm^{-2} s^{-1} for the [OIII]5007 line flux.

2.2. RXJ213807.61-423614.3

The optical spectrum is from the European Southern Observatory 3.6m Telescope. It was obtained in photometric conditions through a 1.5″ slit using EFOSC2 with the 300 lines mm^{-1} grating, yielding 20Å resolution (FWHM measured from arc lines through the same slit). The continuum shape (Fig. 2) is clearly that of a galaxy at $z = 0.019$ with NaI, MgI and CaII absorption lines. A few emission lines can be seen over this continuum, namely [SII]$\lambda\lambda$6732,6717 (badly affected by an atmospheric band), [NII]6584, Hα, [OIII]$\lambda\lambda$ 4959,5007, and probably Hβ, Hγ and [OIII]4363. To get a better estimate of the emission line parameters, we have subtracted the off-nuclear galaxy spectrum to leave only the nuclear component. Now broad Hα can be easily seen, as well as narrow Hβ. We have fitted to this latter spectrum a 5-point spline for the continuum, narrow Gaussians for Hβ, [OIII]$\lambda\lambda$ 4959,5007, [OI]6300, [NII]$\lambda\lambda$6548,6584, Hα, and [SII]$\lambda\lambda$6732,6717, and a broad Gaussian for Hα. Adding a second broad Gaussian at the observed position of Hβ results in $\Delta\chi^2 = 35$ (1004 d.o.f. in total), with an F-test probability of 10^{-7}, so Hβ is detected with high statistical confidence. This source is then a Sy1.8.

The Balmer decrement of the NLR is 3.0 ± 0.4, or in terms of reddening, $E(B-V) = -0.05 \pm 0.12$ (Galactic value of 0.04 already subtracted). The NLR is essentially unreddened. In contrast, the BLR shows a Balmer decrement of 7 ± 1, or $E(B-V) = 0.60 \pm 0.14$.

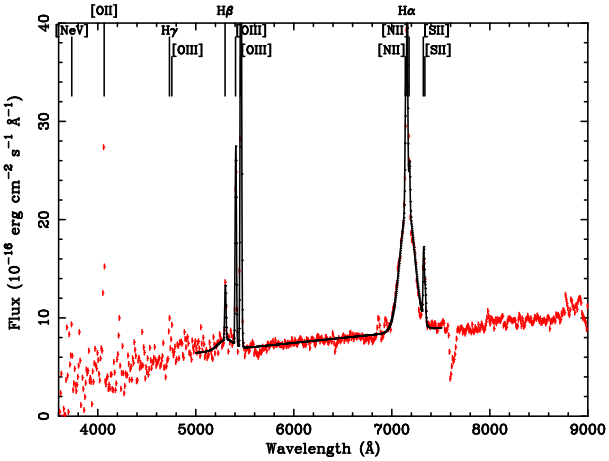

Fig. 1. FOS optical spectrum for RXJ1331, along with the best fit model (over the 5000-7500Å range) including a linear continuum and narrow Gaussian lines for the main emission lines, along with an additional broad Gaussian component for Hα and Hβ (see text for details).

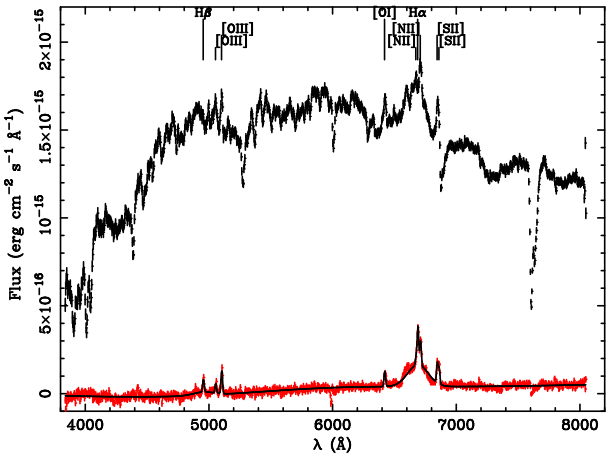

Fig. 2. Optical spectra for RXJ2138: the brightest one is for the nuclear plus galaxy emission, while the fainter one is the galaxy-subtracted nuclear spectrum. We also show the best fit model to the latter, over the whole wavelength range of spectrum. This model includes a five node spline fit to the continuum, narrow Gaussian lines for the main emission lines, and additional broad Gaussians for Hα and Hβ (see text).

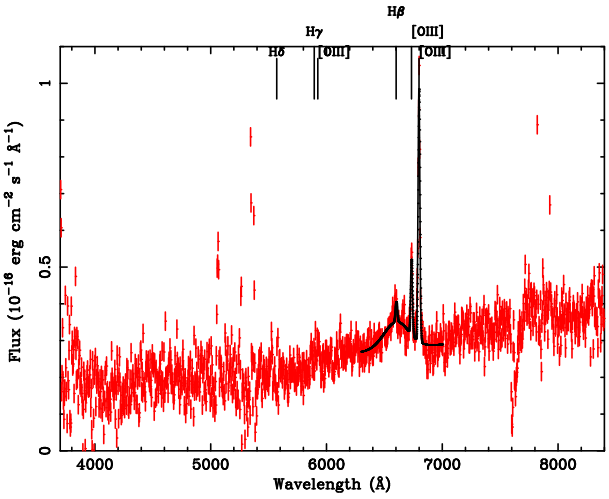

Fig. 3. Optical spectrum for RXJ1630, along with the best fit over the 6300-7000Å range to a linear continuum, narrow Hβ/[OIII] and broad Hβ.

Since the observing conditions were photometric, and the spectrum was obtained through a slit which was 1.5 times the seeing (1 arcsec), we make no photometric correction to the observed [OIII]5007 flux. The [OIII]5007 line arises only from the central ∼arcsecond of the galaxy because its intensity is similar in the nuclear and galaxy+nuclear spectrum (Fig. 2).

2.3. RXJ163054.25+781105.1

This optical spectrum is from the RIXOS survey. It was taken in April 1993 with the ISIS spectrograph at the WHT (see Mason et al. 2000 for details). We show the optical spectrum for this source in Fig. 3, along with the best fit over the 6000-7000Å range to a linear continuum with Gaussian narrow emission lines for [OIII]$\lambda\lambda$4959,5007 and Hβ, and a broad Gaussian component for Hβ as well. The range used to estimate the error bars was 6000-6500Å. Although the centre of the Gaussian representing narrow Hβ does not coincide exactly with the peak of the spectral hump, both components of the Hβ line are significant. Hence we classify this object as a Sy1.5.

The expected position of the Hα line is outside the wavelength coverage of this spectrum, and therefore we cannot measure the Balmer decrement. We can however estimate the amount of reddening from the continuum shape, as explained in section 2.1. Matching the Francis et al. (1991) QSO continuum to this spectrum requires either $N_H \sim (4 \pm 1) \times 10^{21}$ cm^{-2} (much larger than the column density inferred from the X–ray spectrum, see section 3.3) and very little galaxy contribution, or $N_H \sim (0 \pm 1) \times 10^{21}$ cm^{-2} and ∼90% galaxy contribution. Taking into account the presence of galactic absorption lines at the redshift of the source in the optical spectrum, we have chosen this second solution.

To obtain an absolute flux for [OIII]5007 we apply an additional correction factor of 1.9±0.4 based on optical photometry ($R = 18.73 \pm 0.09$), and extrapolating the spectral continuum towards the red using a straight line. This results in an absolute [OIII]5007 line flux of $(0.26 \pm 0.05) \times 10^{-14}$ erg cm^{-2} s^{-1}.

3. *XMM-Newton* observations and data

The spectra reported here come from four different *XMM-Newton* observations (see Table 2) of three different targets. The last target (RXJ1630) was observed twice because in the first observation the `EPIC pn` instrument (the prime instrument of the observation) was off. Most of the observing time for RXJ1238 was lost due to high background caused by a high flux of soft protons.

We processed all the `EPIC` data using `SAS v 5.3.3`. To assemble the source spectra, events in circular regions (36, 20 and 25 arcsec radii for RXJ1331, RXJ2138, and RXJ1630 respectively) around the X–ray source positions were used. These radii were chosen such that the source counts were significantly above the background, so as to maximise the signal to noise ratio of the spectra. Response and effective area files were constructed using the `SAS` tasks rmfgen and arfgen respectively for each source in each instrument and each observation. Background spectra were extracted from several nearby bright-source-free circular regions (avoiding chip gaps in pn). The spectra were constructed from single and double events in pn (pattern≤ 4), and singles, doubles and triples in the MOS (pattern≤ 12).

The spectra from different instruments/exposures for each source were coadded using our own code which also combines the response files. The background spectra were also coadded using the same code, in a way that preserves the statistical properties of the sample, taking into account the different source and background areas for each spectrum. A full description of the recipe used to combine the spectra, backgrounds and response matrices is given in Page, Davis and Salvi (2003). The coadded spectra were binned to have at least 10 counts per bin (RXJ2138 and RXJ1630) or 20 counts per bin (RXJ1331 which

Table 2. Log of *XMM-Newton* observations. The column labelled Target shows both the target name as it appears in the *XMM-Newton* observation log and our shortened names. OBS_ID is the unique *XMM-Newton* observation ID number. Date is the observation date. Texp/Tobs show the final exposure time available for each instrument after cleaning of bad intervals, over the total instrument "on" time.

			Texp/Tobs (s)		
Target	OBS_ID	Date	pn	MOS1	MOS2
278-010/RXJ1331	0061940101	Jan 3, 2001	4174/4651	6969/7039	6983/7043
031-001/RXJ2138	0061940201	Jun 1, 2001	1259/10485	3719/13010	3719/13017
122-013/RXJ1630	0061940301	Sep 20, 2001	-/-	4937/5003	4943/5003
122-013/RXJ1630	0061940901	Apr 11, 2002	1559/7337	4203/9326	4214/9332

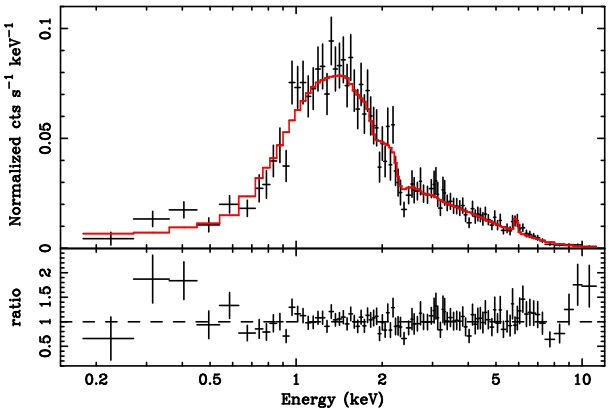

Fig. 4. Spectrum for RXJ1331 (crosses), along with the best fit model (stepped line, including Galactic absorption, redshifted absorption, powerlaw continuum, and a broad emission line). The ratios between the data and the best fit model values are also shown.

has more counts) to allow use of the χ^2 statistic. Only channels with nominal energy between 0.2 and 12 keV were used in the fits.

We have fitted several models (with increasing complexity) to each source, checking at each step the significance of the improvement over the previous fit using the F-test. We have started with a single powerlaw spectrum with absorption by cold gas, with column density fixed at the Galactic value, (models `phabs` and `zpower` in `xspec`). We have then added a second absorption component at the redshift of the source with free column density (`zphabs`), to test for intrinsic absorption. Finally, we have added a Gaussian line with a rest-frame energy of 6.4 keV, and its velocity width fixed to 0, to represent a narrow Fe Kα emission line.

The best fit values are shown in Table 3, and each source is discussed separately below. All uncertainties quoted are 2σ for one interesting parameter.

3.1. RXJ1331

This is the source with the highest flux in our sample, and hence the one with the best X–ray spectrum. The single powerlaw model is a very bad fit. The significance of introducing absorption intrinsic to the source is ∼100%, with an intrinsic column density which is at least ∼20 times the Galactic value. The fit improved (at 99.25%) with the introduction of a narrow Gaussian line at a rest energy of 6.4 keV. The EW is 180 ± 120 eV, which is consistent with values found in nearby, bright Sy1-1.5 (Nandra et al. 1997). This fit is shown in Fig. 4, and its parameters reported in Table 3. We also tried fits in which the width and central energy of the Fe line were free parameters, but these were not significantly better fits to the data (< 99% significance according to the F-test).

Some residuals can be seen between 0.2 and 0.5 keV. We have tried both a partial covering model and a blackbody soft excess to reduce them, but the improvement in the fit was not significant, and obvious residuals still remained in place.

We have tried to fit the X–ray continuum using an ionized absorber. There is no improvement over the neutral gas absorption model (significance ≤ 70%). The best fit powerlaw slope is very similar to the fit with a cold absorber, (1.52 ± 0.11), although the column density is slightly higher ($(50^{+6}_{-11}) \times 10^{20}$ cm^{-2}). However, the ionization parameter is very low ($\xi \sim L/N_e R^2 \sim 0.012^{+0.022}_{-0.012}$). With such an ionization parameter, the abundant elements are at most singly ionized (Kallman & McCray 1982) and hence the absorption detected in RXJ1331 is from cold material.

The residuals above 7 keV prompted us to try a reflection model (Magdziarz & Zdziarski 1995) for this object. The fit to this model with only the relative reflection free, and a Gaussian line with rest energy fixed to 6.4 keV and width fixed to 0 was very good, with $\chi^2 = 84.09$ for 89 d.o.f.. In F-test probability terms this corresponds to an improvement of 99.82% over the cold absorption with no Gaussian line. The EW of the line was 120 ± 110 eV. However, this fit predicted that the reflection component was 9^{+5}_{-2} times the direct component, i.e., this source would be reflection dominated. To check this possibility, we calculated the position of RXJ1331 in the Bassani et al. (1999) diagram. Using the absorption and calibration corrected [OIII]5007 line flux value given in section 2.1, and the source hard flux from Table 3, we get $S_H/F_{[OIII]} = 21 \pm 5$, well into the Compton thin regime in that diagram.

Therefore, the best fit model for this source with the present data is an intrinsically absorbed (but Compton thin) powerlaw with an Fe Kα emission line. The column density obtained from the Balmer decrement of the BLR (under the assumption of standard gas-to-dust ratio), is a factor of >1.5 larger than the value required by the X–ray spectrum. A non-standard gas-to-dust ratio would in principle alleviate this apparent contradiction.

Table 3. Summary of X-ray spectral fits. The values marked with an asterisk (*) are kept fixed in the fit. The values in brackets under the Source column are the intrinsic column densities from fits to the *Rosat* spectra in units of 10^{20} cm^{-2}. F.P. is the F-test probability. The fluxes (S_S and S_H in the 0.5-2 and 2-10 keV bands, respectively) are corrected for Galactic absorption. The luminosities are corrected both for Galactic and intrinsic absorption.

Source	z	$N_{H,Gal}$ (10^{20} cm^{-2})	N_H	Γ	χ^2/ν	F.P. (%)	S_S/S_H (10^{-14} cgs)	$L_{2-10\,\mathrm{keV}}$ (10^{42} cgs)	ϵ_0 (keV)	EW (eV)
RXJ1331	0.090*	1.9*	-	$0.70^{+0.03}_{-0.04}$	543.24/92					
$[63^{+9}_{-8}]$			41^{+7}_{-5}	$1.49^{+0.09}_{-0.10}$	96.95/91	100.0				
			42^{+5}_{-6}	1.51 ± 0.10	88.22/90	99.6	35/176	35	6.4*	180 ± 120
RXJ2138	0.019*	2.6*	-	0.8 ± 0.2	22.33/15					
$[60 \pm 30]$			29^{+45}_{-11}	$1.3^{+0.6}_{-0.3}$	13.19/14	99.2				
			29^{+48}_{-12}	$1.3^{+0.6}_{-0.4}$	13.19/13	-	4/21	0.2	6.4*	0^{+800}
RXJ1630	0.358*	4.1*	-	1.3 ± 0.11	39.97/48					
$[33^{+16}_{-17}]$			12^{+11}_{-8}	1.6 ± 0.2	30.85/47	99.95				
			13^{+11}_{-8}	1.6 ± 0.2	29.73/46	80.6	7/19	72	6.4*	160^{+320}_{-160}

3.2. RXJ2138

With only 17 bins after grouping, this spectrum does not warrant very complex models. A single powerlaw with only Galactic absorption gives a reasonable fit with a very hard powerlaw slope ($\Gamma = 0.8$). The introduction of intrinsic cold absorption improves the fit at > 99%, with a column density of between 6 and ~30 times the Galactic value, though still with a rather hard powerlaw slope ($\Gamma = 1.3$).

The spectrum and model are shown in Fig. 5. An attempt to introduce an additional narrow ($\sigma = 0$) Gaussian line component does not improve the fit, and leaves the other parameters practically unchanged. The upper limit to the EW of the line is 800 eV.

We have used the [OIII] line flux given in section 2.2 and the source hard flux from Table 3 to get $S_H/F_{[OIII]} = 102 \pm 8$. This alone situates this source well into the Compton thin regime in the Bassani et al. (1999) diagram. This source is thus best fitted by an intrinsically hard powerlaw with Compton thin intrinsic absorption. Further components are not required by the data. The absorbing column density deduced from the BLR Balmer decrement is of the order of that required by the X–ray data.

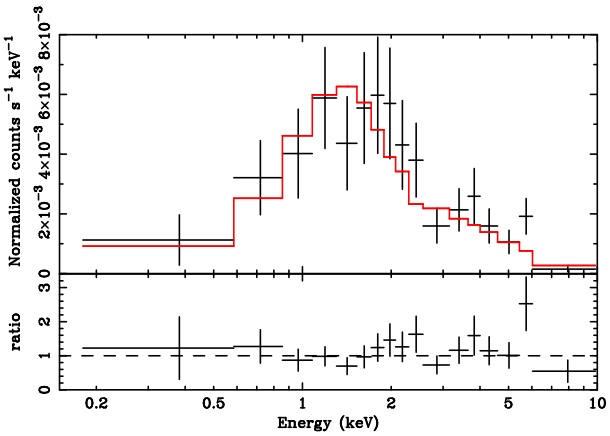

Fig. 5. Spectrum for RXJ2138 (crosses), along with the best fit model (stepped line, including Galactic absorption, redshifted absorption, and a powerlaw continuum). The ratios between the data and the best fit model values are also shown.

3.3. RXJ1630

A fit to a single powerlaw looks reasonable in χ^2 terms, and gives rise to a hard powerlaw. The fit improves at >99.9% if intrinsic absorption is included, with an inferred column density which is between 2 and 6 times the Galactic value. This model is the one shown in Fig. 6.

As in the case of RXJ2138, the introduction of a narrow Gaussian at 6.4 keV does not significantly improve the fit, and the other parameters remain practically unchanged. The upper limit to its EW is 500 eV. We have checked whether this source is Compton thick. From section 2.3 and table 3, its $S_H/F_{[OIII]} = 72 \pm 14$ using the observed [OIII] flux. The source is again well away from the Compton thick region in the Bassani et al. (1999) diagram.

Again, the best model fit to this source is a powerlaw with Compton thin intrinsic absorption. The data do not warrant the introduction of more sophisticated models. The column density deduced from the broad-band optical reddening is within the errors, of the order of the value fitted to the X–ray spectrum.

4. Discussion

The optical spectra of our three AGN define them as intermediate-type Seyferts, with signs of mild (if any) NLR obscuration, but strong BLR obscuration (at least in two of them). Their X–ray spectra are well fitted by relatively hard powerlaws, absorbed by moderate columns (~a few $\times 10^{21}$ cm^{-2}). But, how do the parameters from the X–ray fits compare to those of other AGN at similar fluxes? How does the optical obscuration compare to the X–ray absorption?

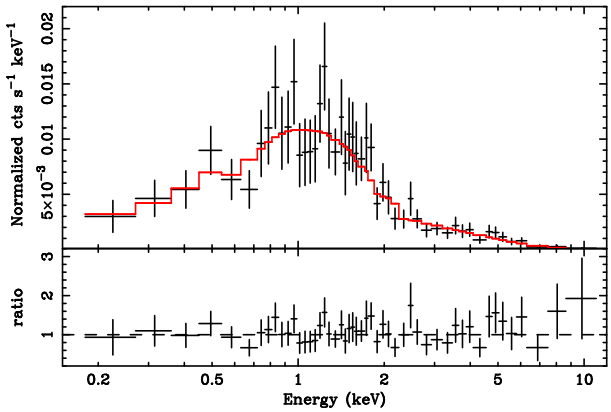

Fig. 6. Spectrum for RXJ1630 (crosses), along with the best fit model (stepped line, including Galactic absorption, redshifted absorption, and a powerlaw continuum). The ratios between the data and the best fit model values are also shown.

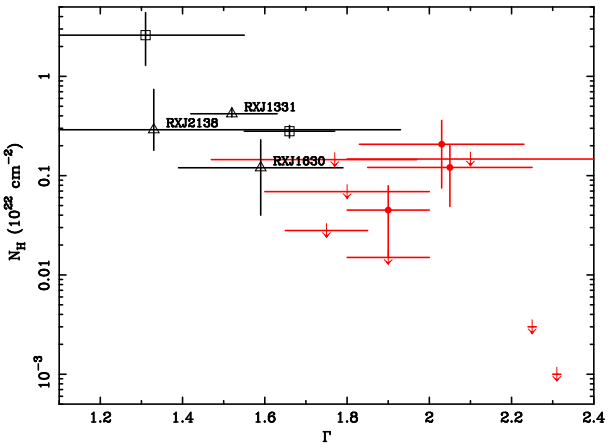

Fig. 7. Intrinsic (redshfited) column density versus powerlaw slope for our hard BLAGN (triangles), and for the 2 BLAGN with significant absorption in Piconcelli et al. (2002) (squares). The AXIS BLAGN with $S_{2-10\,\mathrm{keV}} > 10^{-13}$cgs are also shown, either with solid circles (if the 99% lower limit in column density is > 0), or with arrows pointing down (at the top end of the 99% confidence limits on their column densities). The 90% error bars in the last two samples have been transformed to 95% assuming Gaussian statistics.

4.1. Slope and column density distribution

The intrinsic absorbing column densities from the *XMM-Newton* spectra are between 1.5 and 3 times smaller than those deduced from *Rosat* data (see Table 3 and Page, Mittaz & Carrera 2001). This is probably mainly due to the assumption of $\Gamma = 2$ we had to adopt in that paper because of the limited number of independent bins in the *Rosat* spectra. In all three cases the *XMM-Newton* spectra show that our sources have intrinsically somewhat flatter spectra than $\Gamma = 2$.

To examine how our sources relate to the wider AGN population, we have compared the powerlaw slopes and column densities of our sources to those of other AGN with broadband ($\sim 0.5 - 10$ keV) X–ray spectra.

Significant samples of bright Seyferts have been observed with *ASCA* and form a good benchmark with which to compare our sources. George et al. (1998) studied the *ASCA* X–ray spectra of a sample of 18 nearby Sy1-1.5. Two objects in their sample showed significant instrinsic absorption: IC4329A, has $N_H \sim 4 \times 10^{21}$ cm^{-2} (of the order of the N_H found for RXJ1331), and NGC4151 has a larger N_H of up to a few $\times 10^{22}$ cm^{-2} (see also Schurch & Warwick 2002). Only 3 of these 18 Sy1-1.5 have best-fit power law slopes which are as hard or harder than those of our *Rosat* selected sources. Our hard sources appear to have flatter slopes and much higher absorption than unobscured Sy1-1.5 of equal or higher X-ray luminosities. However, photoelectric absorption is more frequently discernable in the X–ray spectra of Seyferts with higher levels of optical obscuration. In a sample of 25 bright Sy1.9-2 observed with *ASCA*, Turner et al. (1997) found significant cold absorption in 14 objects, of which 12 are more heavily absorbed that our *Rosat* selected objects. In contrast to the Sy1-1.5, almost half of these sources (11/25) have best-fit spectral slopes as hard, or harder, than our sources. Our hard sources seem to have similar slopes but lower absorption than obscured Sy1.9-2 of similar X-ray luminosities.

At 2-10 keV flux levels more similar to our three *Rosat* selected sources, we can draw a comparison sample from the serendipitous *XMM-Newton* sources of Mateos et al. (2003a), based on the AXIS project (Barcons et al. 2002). In that sample there are 9 broad line AGN with 2-10 keV fluxes $\geq 10^{-13}$ cgs showing broad optical/UV emission lines whose spectra have been modelled with a powerlaw and intrinsic cold absorption (Mateos et al. 2003b). We show in Fig. 7 the best fit parameters for those sources, along with those for our three *Rosat* selected sources. Three of the AXIS broad line AGN show significant absorption, with similar column densities to those found in our sources, but softer power law slopes than our three objects. On the other hand, the two broad line AGN in the 2-10 keV selected sample of *XMM-Newton* sources from Piconcelli et al. (2002), for which there is evidence for intrinsic absorption, have similar powerlaw slopes, and similar or higher column densities to our sources (see also Fig. 7).

Inevitably, the comparison is subject to small number statistics, compounded by the fact that none of the samples discussed (including ours) can be said to be complete in a statistical sense. It is therefore not clear whether the hard-spectrum *Rosat* survey has selected sources with a different (flatter) distribution of power law slopes to the 2-10 keV population as a whole. However, it does appear that objects with intrinsic column densities of a few $\times 10^{21}$ cm^{-2} are an important part of the moderately bright ($\geq 10^{-13}$ cgs) 2-10 keV AGN population.

4.2. Optical obscuration and X–ray absorption

Our three objects show intrinsic absorption in their X–ray spectra, well above that expected from material in our Galaxy. Furthermore, the very low Balmer decrement in the NLR of RXJ1331 and RXJ2138 imply that this absorption is intrinsic to the nuclei of these objects, and not due to extra-nuclear material in their host galaxies.

The Balmer decrement on the BLR of RXJ2138 is larger than we would expect from the best fit X–ray column density (if we assume a Galactic gas-to-dust ratio and extinction curve), although the two measurements are compatible because of the relatively large uncertainty on the X–ray column density. Under this assumption, the optical reddening from the continuum shape of RXJ1630 and its best fit X–ray column density are also compatible (within the errors). This is not the case for RXJ1331, in which the Balmer decrement from the BLR corresponds to a cold gas column density 1.5 times higher than that deduced from fits to its X–ray spectrum, under that assumption.

An apparent excess of optical redenning compared to X–ray photoelectric absorption, as observed in RXJ1331, has already been observed in several other AGN. For example, the Sy1.8/1.9 galaxy H1320+551 (Barcons, Carrera & Ceballos 2003) has a BLR Balmer decrement ($(H\alpha/H\beta)_{BLR} > 27$), but no signs of significant intrinsic absorption in its Compton thin X–ray spectrum. Pappa et al. (2001) also find a couple of cases of optically obscured Sy2 galaxies with no signs of X–ray absorption. These authors propose three possible reasons for the mismatch of optical obscuration and X–ray absorption: (a) the BLR does not exist or is intrinsically reddened; (b) the sources are Compton thick, and the flux below 10 keV is due to scattered or host galaxy emission; (c) a dusty warm absorber reddens the BLR but does not affect much the X–ray properties.

We have already discarded possibility (b) for all three of our AGN, based on the Bassani et al. (1999) diagram. We can also discard (c) for RXJ1331, as a warm absorber is not consistent with the data. RXJ1331 is therefore an intriguing object. It has a small reddening of the NLR (situating the absorbing material closer to the nucleus than the NLR), no evidence for a warm absorber, and a strong mismatch between the optical BLR Balmer decrement and X–ray absorption. Could it be then that some component of the large BLR Balmer decrement is intrinsic to the BLR and is not due to optical redenning along the line of sight?

To answer this question, we have compared the properties of RXJ1331 with those of the sample of Seyfert galaxies of Ward et al. (1988), who find a good correlation between the Balmer decrement and the 2-10 keV to Hβ ratio (see appendix A). RXJ1331 has a Balmer decrement ∼0.4 dex above what would be expected from its 2-10 keV to Hβ ratio, and the Ward et al., correlation. Changing the gas-to-dust ratio would not bring RXJ1331 into line with the Seyfert galaxies in Ward et al. (1988): the reddening vector in Fig. 4 of Ward et al. (1988) is parallel to their observed correlation. This might suggest that RXJ1331 is therefore similar to, though much less extreme than, H1320+551, which shows no significant absorption to either its X–ray or optical continua despite its very large Balmer decrement.

However, the non-simultaneity of our X-ray observation (2001) and optical spectrum (1994) could also be responsible for the discrepancy. RXJ1331 was discovered serendipitously in the *Rosat* observation with ROR number rp701034n00 (done on July 18, 1992), with a countrate in the 0.1 to 2.4 keV band of 0.037±0.002 and hardness ratios HR1=0.97±0.04 and HR2=0.68±0.05. It also appears in the *Rosat* All Sky Survey (performed in the first half year of the ROSAT mission in 1990-1991) Bright Source Catalogue (RASSBSC, Voges et al. 1999) with a countrate of 0.10±0.02 in the same band, and hardness ratios HR1=1.00±0.14 and HR2=0.65±0.20. For comparison, we have taken the best fit model to the *XMM-Newton* spectrum of RXJ1331 and used `xspec` to calculate the expected count rates for *Rosat*, obtaining a total countrate of 0.025±0.002, and hardness ratios HR1=0.98 and HR2=0.65. RXJ1331 thus presents remarkably stable X-ray spectral properties over a 10 year period, but has varied in intensity such that it was a factor 4 brighter when observed in 1990/1991 than in 2001. If RXJ1331 was as bright in X-rays in February 1994 when its optical spectrum was recorded as it was during the *Rosat* All Sky Survey, it is relatively consistent with the Ward et al (1988) sample, and its Balmer decrement can be explained by a higher than Galactic dust-to-gas ratio. If instead, it was at a similar X-ray flux level to those observed in 1992 and 2001, it is a more complex object, similar to, though much less extreme than, H1320+551.

We have found that the three X–ray brightest broad line AGN from the hard-spectrum *Rosat* survey have optical reddening similar to, or larger than, would be expected for an absorber with a Galactic gas-to-dust ratio and reddening law. This finding is particularly interesting because it is contrary to what has been found for the majority of X–ray absorbed AGN studied so far. For example, in our own survey (Page, Mittaz & Carrera 2000) we found a total of 13 $z > 1$ hard spectrum luminous BLAGN of which 10 have $\log(N_H/cm^{-2}) \geq 22$. If "effective" gas-to-dust ratios as large as the ones we have found for RXJ1331, RXJ1630 and RXJ2138 were present in those high redshift AGN, the amount of optical obscuration would be sufficient to completely block the BLR ($E(B-V) \sim 7-13$ for their mean $\log(N_H/\mathrm{cm}^{-2}) \sim 22.29$). This is certainly not the case, because broad emission lines are detected in all of them. An equally good demonstration of this point is the study of Maiolino et al. (2001), who constructed a sample of AGN with measurements of both optical reddening and X–ray photoelectric absorption. The $E(B-V)/N_H$ value was found to be significantly lower than Galactic in 16 out of the 19 objects studied. The other 3 objects in their study were all low luminosity objects (2-10 keV luminositiy $< 10^{42}$ cgs). Our *XMM-Newton* observations show that ≥Galactic $E(B-V)/N_H$ values *can* be found in more luminous objects (e.g. RXJ1630 has a 2-10 keV luminosity of 7×10^{43} cgs), although this may be much rarer in such sources.

It appears that the luminous AGN which are abundant at high redshift cannot simply be scaled-up versions of the low redshift AGN presented here. There must be some other ingredient, such us a luminosity dependence or evolutionary effect in the gast-to-dust contents of the absorber which gives rise to the different absorption characteristics in high and low redshift AGN.

5. Conclusions

We have presented X–ray spectra from *XMM-Newton* of the three brightest AGN exhibiting broad optical emission lines (all three are intermediate Seyferts) from the sample of hard spectrum *Rosat* sources (Page, Mittaz & Carrera 2000, 2001). The

X–ray spectra of all three sources are well fitted by powerlaws ($\Gamma \sim 1.5$), absorbed by moderate amounts of intrinsic nuclear cold material ($N_{\rm H}$ ~a few $\times 10^{21}$ cm^{-2}). Similarly absorbed sources are an important part of the $S_{2-10\,{\rm keV}} \geq 10^{-13}$ cgs AGN population, although the three sources studied here appear to have harder intrinsic power law slopes than the majority of AGN at this flux level.

The equivalent width of the narrow emission line at about 6.4 keV found in RXJ1331 is typical of other radio-quiet Compton-thin Seyferts.

Detailed analysis of our optical spectroscopic data confirm the classification of these sources as intermediate-type Seyfert galaxies (Sy1.5-Sy1.9). For the two objects in which both Hα and Hβ are visible (RXJ1331 and RXJ2138), the NLR is shown to be almost free of reddening, while the BLR is significantly reddened. The column density necessary to produce this effect is about 1.5 times that inferred from the X–ray absorption in RXJ1331, and of the order of it in RXJ2138 and RXJ1630 (in this last case from its broad band optical spectrum), if standard Galactic gas-to-dust ratios are assumed.

None of the three sources are Compton-thick. The X–ray data for RXJ1331 require that the absorber is cold, allowing us to rule out the presence of dust embedded in a warm absorber in this source.

These three low redshift broad line AGN from our sample of hard sources show a ratio of optical extinction to X–ray absorption which is similar to, or larger than, the interstellar medium of our own Galaxy. This cannot be the case for the high luminosity, high redshift, broad line AGN in our sample, because the broad lines would be completely obscured at the X–ray column densities ($> 10^{22}$ cm^{-2}) observed in these sources.

To explain the whole population of absorbed AGN, their effective gas-to-dust ratio must show a large variety, perhaps depending on luminosity, evolving with redshift, or showing geometries different from those proposed by the unified AGN model.

Acknowledgements. We thank the anonymous referee for useful remarks. The work reported herein is based partly on observations obtained with *XMM-Newton*, an ESA science mission with instruments and contributions directly funded by ESA member states and the USA (NASA). This research was based partly on observations collected at the European Sourhern Observatory, Chile, ESO No. 62.O-0659. The WHT and INT telescopes are operated on the island of La Palma by the Issac Newton Group of Telescopes in the Spanish Observatorio del Roque de Los Muchachos of the Instituto de Astrofísica de Canarias. Partial financial support for this work was provided by the Spanish Ministry of Science and Technology under project AYA2000-1690.

References

Akiyama M., Ohta K., Yamada T., et al., 2000, ApJ, 532, 700
Antonucci R., 1993, ARA&A, 31, 473
Barcons X., Carrera F.J., Watson M.G., et al., 2002, A&A, 382, 522
Barcons X., Carrera F.J., Ceballos M.T., 2003, MNRAS, 339, 757
Bassani L., Dadina M., Maiolino R., Salvati M., Risaliti G., Della Ceca R., Matt G., Zamorani G., 1999, ApJ, 121, 473
Bohlin R.C., Savage B.D., Drake J.F., 1978, ApJ, 224, 132
Brandt W.N., Fabian A.C., Pounds K.A., 1996, MNRAS, 278, 326
Brotherton M.S., Tran H.D., Becker R.H., Gregg M.D., Laurent-Muehleisen S.A., White R.L., 2001, ApJ, 546, 775
Carrera F.J., Page M.J., Stevens J.A., 2003, ESA SP-488, in press
Coleman G.D., Wu C.C., Weedman D.W., 1980, ApJS, 43, 393
Ferguson J.W., Ferland G.J., 1997, ApJ, 479, 363
Fiore F., La Franca F., Giommi P., Elvis M., Matt G., Comastri A., Molendi S., Gioia I., 1999, MNRAS, 306, L55
Francis P.J., Hewett P.C., Foltz C.B., Chafee F.H., Weymann R.J., Morris S.L., 1991, ApJ, 373, 465
Francis P.J., 2003, `http://msowww.anu.edu.au/~pfrancis/composite/`
George I.M., Turner T.J., Netzer H., Nandra K., Mushotzky R., Yaqoob T., 1998, ApJS, 114, 73
Gilli R., Salvati M., Hasinger G., 2001, A&A, 366, 407
Granato G.L., Danese, L., Franceschini A., 1997, MNRAS, 486, 147
Kallman T.R., McCray R., 1982, ApJS, 50, 263
Lehman I., Hasinger G., Schmidt M., et al., 2001, A&A, 371, 833
Magdziarz P., Zdziarski A.A., 1995, MNRAS, 273, 837
Mainieri V., Bergeron J., Hasinger G., Lehmann I., Rosati P., Schmidt M., Szokoly G., Della Ceca R., 2002, A&A, 393, 425
Maiolino R., et. al., 2001, A&A, 365, 28
Maiolino R., Marconi A., Oliva E., 2001, A&A, 365, 37
Mason K.O., Carrera F.J., Hasinger G., et al., 2000, MNRAS, 311, 456
Mateos S., Barcons X., Carrera F.J., Ceballos M.T., et al., 2003a, AN, 324, 48
Mateos S., Barcons X., Carrera F.J., Ceballos M.T., 2003b, in preparation
Mushotzky R.F., Ferland G.J., 1984, ApJ, 278, 558
Nandra K., Pounds K.A., 1994, MNRAS, 268, 405
Nandra K., George I.M., Mushotzky R.F., Turner T.J., Yaqoob T., 1997, ApJ, 477, 602
Netzer H., Elitzur M., Ferland G.J., 1985, ApJ, 299, 752
Osterbrock D.E., 1989, Astropysics of Gaseous Nebulae and Active Galactic Nuclei, University Science Books, Mill Valley, CA
Page M.J., Mittaz J.P.D., Carrera F.J., 2000, MNRAS, 318, 1073
Page M.J., Mittaz J.P.D., Carrera F.J., 2001, MNRAS, 325, 575
Page M.J., McHardy I.M., Gunn K.F., et al., 2003, AN, 324, 101
Page M.J., Davis S.W., Salvi N.J., 2003, MNRAS, 343, 1241
Panessa F., Bassani L., 2002, A&A, 394, 435
Pappa A., Georgantopoulos I., Stewart G.C., Zezas A.L., 2001, MNRAS, 326, 995
Piconcelli E., Cappi M., Bassani L., Fiore F., Di Cocco G., Stephen J.B., 2002, A&A, 394, 835
Rees M.J., Netzer J., Ferland G.J., 1989, ApJ, 347, 640
Richards G.T., et al., 2003, AJ, 126, 1131
Schurch N.J., Warwick R.S., 2002, MNRAS, 334, 811
Setti G., Woltjer L., 1989, A&A, 224, L21
Smith D., Done C., 1996, MNRAS, 280, 335
Turner T.J., George I.M., Nandra K., Mushotzky R.F., 1997, ApJS, 113, 23
Vanden Berk D.E., et al., 2001, AJ, 122, 549
Ward M.J., Done C., Fabian A.C., Tennat A.F., Shafer R.A., 1988, ApJ, 324, 767

Appendix A: Estimating the optical obscuration

When available, we have used the Balmer decrements (Hα/Hβ) to calculate the extinction. The standard unreddened Balmer decrement is (Hα/Hβ) = 3 (Osterbrock 1989), as expected for case B recombination and optically thin gas. This is expected to hold for the NLR, but there are several theoretical reasons why

case B recombination might not apply to the BLR, because of the high density of the clouds in this region. Collisional, self-absorption and radiative transport effects can affect the Balmer decrement, which can have values between about 1 and 20, depending on the exact (and largely unknown) physical state of the matter in the BLR clouds, as shown by many theoretical works and calculations (e.g. Mushotzky & Ferland 1984, Netzer, Elitzur & Ferland 1985, Rees et al. 1989, Ferguson & Ferland 1997).

To estimate the typical intrinsic Balmer decrement in AGN we have analyzed the region between 4600 and 7000 Å of several composite optical QSO spectra, following the same procedure we have followed for the spectra of our sources, as outlined above. The templates have BLR Balmer decrement values around 3 (FIRST Bright QSO Survey -Brotherton et al. 2001-: 2.53 ± 0.04, SDSS -Vanden Berk et al. 2001-: 2.38 ± 0.04, Large Bright QSO Sample and others -Francis 2003-: 3.36 ± 0.09), in any case well below the most extreme values in the above theoretical calculations.

In a different approach, Ward et al. (1988) have measured the average intrinsic unreddened Hα/Hβ ratio in the BLR of a sample of 46 AGN (including Sy1 to Sy1.9, broad-line radio galaxies and quasars) to be 3.5, independent of any atomic physics assumptions. They found a good linear corretion in the log space (see their Fig. 4) between the BLR Balmer decrement, and the ratio of 2-10 keV luminosity $L_{2-10\,\mathrm{keV}}$ (practically unaffected by Compton thin absorption), to Hβ luminosity (strongly dependent on absorption). This led them to suggest that the Balmer decrement is determined by nuclear reddening, rather than being intrinsic to the BLR. By fitting a straight line to this correlation, they find that the AGN reddening law between about 4900 and 6600Å is similar to that in our Galaxy, and they relate the intrinsic $L_{2-10\,\mathrm{keV}}$/Hβ ratio to the intrinsic Balmer decrement. They determine the intrinsic $L_{2-10\,\mathrm{keV}}$/Hβ ratio from a subsample of their sources deemed to be subject to very little reddening, obtaining finally a value of Hα/Hβ=3.5 (see Ward et al. 1988 for details). We have repeated their analysis including the uncertainties in the fitted parameters, obtaining Hα/Hβ=3.43±0.19, again very similar to the standard value of 3.

We will therefore use Hα/Hβ=3.43±0.19 as an estimate of the intrinsic unreddened Balmer decrement value in the BLR of X-ray AGN, since this value has been obtained from a sample of X-ray AGN with a similar X-ray luminosity range as our sources (see Table 3, and Table 1 of Ward et al. 1988), and independently of any atomic physics assumptions.

We have also compared the broad-band optical spectral shape of RXJ1630 (for which no BLR Balmer decrement can be obtained) with that of the composite QSO spectrum from Francis (2003), with some contribution from a galaxy continuum (in our case we have tried an ES0 from the Coleman, Wu & Weedman 1980 model). The broad-band continuum slopes of the three QSO templates cited above are different, as is that from Francis et al. (1991), with the spectrum from Francis (2003) being the flattest and that from Francis et al. (1991) being the steepest. Over the rest frame range 3800 to 8500 Å, the differences between these two extreme examples can be parameterized as reddening by a Galactic law with $E(B-V) = 0.17$. This is the uncertainty we will assign to the reddening determined from the broad-band optical spectral shape.

Estimating the reddening in this fashion could be misleading if the sources happen to have an intrinsically "red" continuum. Richards et al. (2003) have studied the overall continuum and emission line properties of quasars from the SDSS, finding that there is a population of intrinsically red quasars. They have produced composite spectra of their "normal" quasars in four relative optical magnitude bins, and estimated the slope of the optical continuum α_ν ($f(\nu) \propto \nu^{\alpha_\nu}$) to be between ∼-0.25 and -0.76. Taking the line-free regions recommended by Vanden Berk et al. (2001) (1350-1365 Å and 4200-4230 Å), we have estimated the slope of the Francis (2003) composite spectrum to be $\alpha_\nu = -0.97$, falling with ν faster than any of the Richards et al. (2003) "normal" quasars. Since the slope of the Francis et al. (1991) spectrum is $\alpha_\nu = -0.35$, we conclude that our estimate of the reddening from the optical continuum is conservative both in absolute value (because we are using a spectrum with an "intrinsically" red continuum), and in the assigned uncertainty (because it includes a very broad range of continuum spectral shapes).